diffusion-fundamentals.org

The Open-Access Journal for the Basic Principles of Diffusion Theory, Experiment and Application

Hot Brownian motion and photophoretic self-propulsion

Romy Schachoff[1], Markus Selmke[1], Andreas Bregulla[1], Frank Cichos[1], Daniel Rings[2], Dipanjan Chakraborty[2,3], Klaus Kroy[2#], Katrin Günther[4], Anja Henning-Knechtel[4], Evgeni Sperling[4], Michael Mertig[4,5§]*

[1]Institute for Experimental Physics I, Universität Leipzig, Leipzig, Germany

[2]Institute for Theoretical Physics, Universität Leipzig, Leipzig, Germany

[3]Dep. of Physical Sciences, Indian Institute of Science Education and Research Mohali, Punjab, India

[4]Physikalische Chemie, Mess- und Sensortechnik, Technische Universität Dresden, Germany

[5]Kurt-Schwabe-Institut für Mess- und Sensortechnik e.V. Meinsberg, Waldheim, Germany

*cichos@physik.uni-leipzig.de, [#]klaus.kroy@uni-leipzig.de, [§]michael.mertig@tu-dresden.de

Abstract

We describe the motion of heated particles in a simple liquid, for which we can theoretically derive generalized fluctuation-dissipation relations that hold far from equilibrium, as we demonstrate both experimentally and via molecular-dynamics simulations. Due to persistent laser-light absorption, these particles excite a radially symmetric or asymmetric (Janus particles) temperature profile in the solvent, which affects their random (Brownian) and systematic (self-phoretic) motion. In case of a radially symmetric temperature profile, we show that the particles perform “hot Brownian motion” (HBM), with different effective temperatures pertaining to their various degrees of freedom. We moreover predict and experimentally observe a peculiar dependence of their diffusivity on the particle size. In case of an asymmetric temperature profile, we find a superimposed self-phoretic directed motion. To adjust the importance of this “active” motion relative to the random hot Brownian motion, the shape of the particle is modified by binding DNA molecules and DNA origami to Janus beads. The persistence of the directed transport can thereby greatly be enhanced.

Keywords: Hot Brownian motion, self-thermophoresis, Janus particles, DNA-templated micro-swimmers

1 Introduction

Microscopically, temperature is often deduced from the kinetic energy stored in the velocity degrees of freedom of atoms or molecules. For the overdamped motion of colloidal particles suspended in a fluid, the kinetic energy is constantly dissipated into heat, which is readily turned back into motion via the fluctuations of the hydrodynamic solvent velocity field. This concept of fluctuation and dissipation is well explored in thermal equilibrium. In the form of the Stokes–Einstein relation, it allows the temperature

and certain transport properties of the fluid to be deduced from the Brownian fluctuations of suspended probes. In non-isothermal situations, for example for a laser-heated Brownian particle, such fluctuation dissipation relations have so far not been known. We have baptized the non-equilibrium thermal motion of nanoparticles suspended in a fluid and persistently heated beyond the ambient temperature “hot Brownian motion” (HBM). A typical realization is provided by metal nanoparticles diffusing in the focus of a laser beam. The heat flux into the surrounding solvent caused by the optical heating quickly establishes an essentially co-moving temperature and viscosity profile in the solvent around the particle, as depicted in Figure 1. Below, we show that the non-equilibrium Brownian motion of the particle allows for an effective equilibrium description in terms of a fictitious particle in an isothermal solvent with an effective temperature and viscosity that can explicitly be calculated from our theory [1–4].

Interestingly, the various degrees of freedom of the particle (e.g., for a sphere, translational and rotational positions and momenta) are each predicted to have their own effective temperatures, which is a manifestation of the fact that the system is very far from equilibrium. The characterization of the motion by these effective temperatures and friction coefficients allows the judicious application of the effective equilibrium theory in many situations of fundamental and practical interest, such as the motion of hot particles in external fields and confinement, without resorting to laborious full-scale simulations.

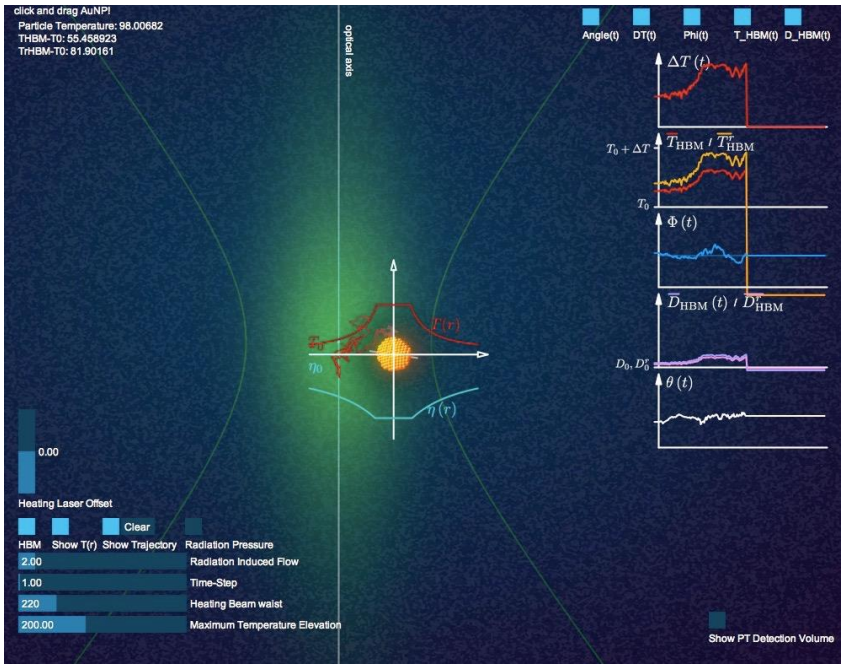

Figure 1: Animation illustrating the physics of hot Brownian motion [1] (program written by M. Selmke). A gold nanoparticle is exposed to laser light (of spatially variable intensity), which is partially absorbed. As a consequence, a persistent heat flux to the surroundings is excited that creates co-moving spatial temperature and viscosity profiles in the solvent (red/blue curves above and below the particle). The HBM-theory underlying the animation maps the non-equilibrium Brownian motion of the heated particle onto the equilibrium Brownian motion of a fictitious isothermal Brownian particle with effective temperatures for its rotational and translational motion, and corresponding effective friction coefficients and diffusivities (inserted graphics). All these quantities can analytically and explicitly be calculated from the underlying non-equilibrium fluctuating hydrodynamics [2–5].

We have not only derived a number of new theoretical predictions for hot Brownian motion, we have also tested them both experimentally, using laser-heated gold nanoparticles in water, and numerically, using non-equilibrium molecular dynamics simulations of solid nanoparticles suspended in a Lennard-

Jones fluid. With some effort, both procedures could indeed be sufficiently refined to allow for parameter-free comparison of theory and measured experimental and numerical data, with excellent success [2, 6] (see Figure 3).

We have moreover analyzed more complicated situations involving thermally anisotropic particles that perform a directed self-phoretic motion. Their preparation, experimental study, numerical simulation, and theoretical description provide substantial challenges, beyond those encountered for hot Brownian particles. Various designs of these anisotropic particles have been tested, by hybrid designs combining Janus beads with DNA and DNA origami. Thereby, we managed to tune the directional persistence of the self-propelled motion in a wide range.

2 Theory and experimental realization of hot Brownian motion

The particle's Brownian motion is affected by the temperature rise generated by the particle in the surrounding solution. This temperature rise is a result of the absorbed and released optical energy by the particle and thus relates to the absorption cross section of the particle by

$$\Delta T = \frac{P_{\mathrm{heat}}}{4\pi\kappa R} = \frac{I_{\mathrm{heat}}\sigma_{\mathrm{abs}}(R)}{4\pi\kappa R}. \tag{1}$$

Here I_{heat} is the intensity of the heating laser in the particles plane, σ_{abs} is the absorption cross-section, κ is the surrounding medium's heat conductivity and R is the particle radius. When keeping the incident heating laser intensity constant, the temperature rise ΔT will thus scale with the inverse particle radius and the absorption cross section. The absorption cross section itself is in general a function of the particle size. In the range up to about 30 nm particle radius, the absorption cross section scales with the volume and particles can be treated as Rayleigh scatterers. Above 30 nm radius, the absorption cross section deviates from the volume dependence since the radiation cannot penetrate the full particle volume. Therefore the temperature rise of the particle in water shows a characteristic maximum at about 60 nm radius (see Figure 2). This has important consequences on the motion of heated particles, since both the viscous friction and the driving thermal fluctuations in the liquid depend on the fluid temperature in the surroundings of the particle.

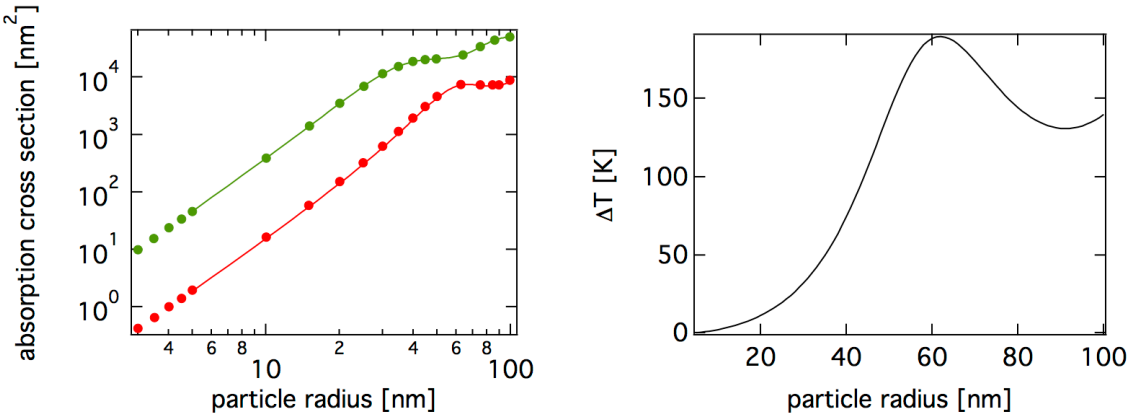

Figure 2: Size dependence of the absorption cross section (left) from Mie calculations [7] at 532 nm (green) and 635 nm (red) and the temperature rise of gold nanoparticles in water of different size (right).

diffusion-fundamentals.org 23 (2015) 1, pp 1–19

Via both effects the heating contributes to the translational and rotational Brownian motion of a heated particle. The notion of hot Brownian motion for this type of non-isothermal Brownian motion emphasizes its non-equilibrium character [1]. It turns out that for a Markovian description of HBM (pertaining to times that are much longer than the decay of the long-time tails), the non-equilibrium effects can be subsumed into a small number of effective transport coefficients that can analytically and explicitly be calculated: chiefly, an effective reduced solvent viscosity η_{HBM} and an effective temperature T_{HBM}. The two quantities determine the effective diffusivity D_{HBM} via a generalized Stokes–Einstein relation. To estimate the viscous friction, the equation of state $\eta(T)$ of the solvent must be known. If we represent it by a Vogel Fulcher law, $\eta(T) = \eta_\infty \exp(A/(T - T_{\mathrm{VF}}))$ as appropriate for water, we can obtain an explicit accurate prediction for the effective translational friction coefficient of the hot particle in terms of an apparent effective solvent viscosity given by

$$\frac{\eta_0}{\eta_{\mathrm{HBM}}} = 1 + \frac{193}{486}\left[\ln\frac{\eta_0}{\eta_\infty}\right]\theta - \left[\frac{56}{243}\ln\frac{\eta_0}{\eta_\infty} - \frac{12563}{118098}\ln^2\frac{\eta_0}{\eta_\infty}\right]\theta^2 + O(\theta^3). \tag{2}$$

A similar (but practically less important since hardly detectable) result can be derived for the renormalization of the effective rotational friction.

Practically and conceptually more important is the effective temperature that characterizes the thermal agitation of the hot Brownian particle:

$$T_{\mathrm{HBM}} = \frac{\int \phi(r) T(r) \mathrm{d}^3 r}{\int \phi(r) \mathrm{d}^3 r}. \tag{3}$$

It is determined from the condition that it characterizes the Brownian motion of the heated diffusing particle as if it were an equivalent isothermal particle. Here $\phi(r)$ is the so-called dissipation function which depends on the viscosity and the solvent velocity gradient and weighs the importance of fluctuations at various local temperatures $T(r)$ according to their relevance for the agitation of the Brownian particle. This prescription leads to different effective temperatures

$$T_{\mathrm{HBM}}^{\mathrm{rot}} \approx T_0\left(1 + \frac{3}{4}\frac{\Delta T}{T_0}\right) \tag{4}$$

and

$$T_{\mathrm{HBM}}^{\mathrm{trans}} \approx T_0\left(1 + \frac{5}{12}\frac{\Delta T}{T_0}\right) \tag{5}$$

characterizing the rotational and translational Brownian motion of the particle, respectively. Higher order terms that involve the effective viscosity can be calculated but are usually small in actual applications [5]. Together with the above renormalized friction, the translational effective temperature determines the generalized Stokes–Einstein relation for the observed diffusivity of a hot Brownian particle, and a similar result holds for the rotational diffusion.

We could validate these – at first sight somewhat unintuitive – predictions experimentally and in numerical simulations, as demonstrated below (see Figure 3).

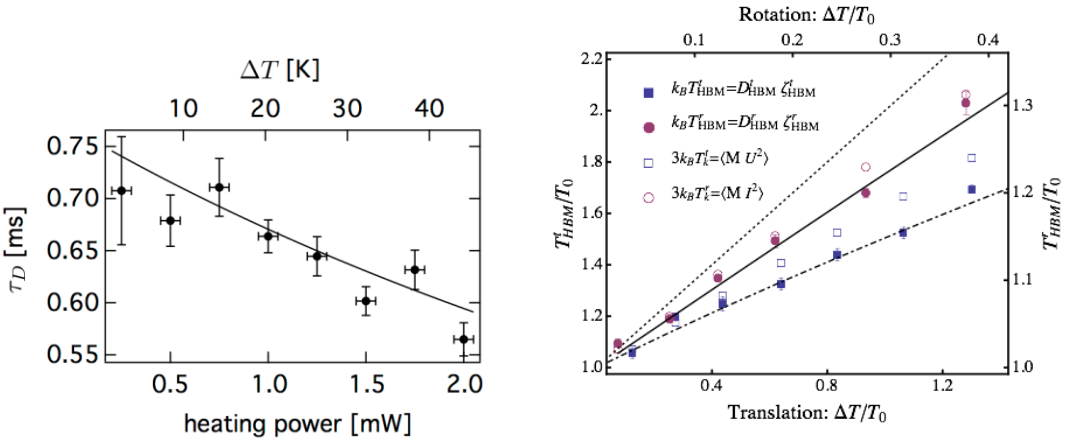

Figure 3: (left) Experimental test of the predicted diffusivity of a hot Brownian particle by the Twin-PhoCS method. The plot displays the measured average time needed by a hot Brownian particle to cross the laser focus and a parameter-free comparison with the theoretical prediction [6]. (right) Parameter-free comparison of the theoretical predictions for the hot Brownian motion of a spherical nanoparticle with results from NEMD simulations. The plot displays the apparent effective temperatures for the rotational and translational hot Brownian motion of a nanoparticle dissolved in a Lennard-Jones fluid (see Figure 8) as deduced from the generalized Stokes–Einstein relations (predicted by the theory and verified by the simulations) in comparison with the analytically calculated results. Also included are the simulation results for the effective hot Brownian kinetic temperatures that pertain to the corresponding kinetic degrees of freedom (rotational and translational velocities). For these quantities, we have only recently obtained theoretical predictions applicable to incompressible solvents [4]. These predictions could so far neither been tested experimentally, nor have the results been generalized to highly compressible solvents, as would be necessary for a comparison with the shown simulation results, due to considerable technical difficulties encountered in of both tasks.

3 Photothermal correlation spectroscopy

To detect the motion of heated nanoparticles in a liquid, photothermal single particle correlation spectroscopy has been developed. Photothermal single particle microscopy employs the heat released by an absorbing particle to generate a local refractive index change in the surrounding liquid. The changed refractive index profile follows the temperature profile generated by the particle, which is long ranged and decays with the inverse distance from the particle. Due to this long-range character, very small particles and even single molecules can be detected [8–10].

The experimental photothermal microscopy setup employs two laser beams, which are focused into the sample plane by a high numerical aperture objective. One of the laser beams (532 nm) is nearly resonant with the particles peak absorption wavelength. This laser is modulated sinusoidally in intensity at a frequency of 300 kHz by an acousto-optical modulator [10]. The second laser beam, which is off-resonant with the absorption of the nanoparticles (635 nm) is focused into the same region. This laser is scattered from the generated refractive index change and thus picks up a modulation at the frequency of the heating laser. The modulation amplitude and phase with respect to the heating laser is analyzed by a lock-in amplifier and recorded by a real time data logging board. For photothermal correlation spectroscopy (PhoCS) [11], recording is carried out with a time-constant of 50 µs.

The overlap of both heating and detection laser is accurately adjusted with the help of scattering images of individual gold nanoparticles at low laser power. The overlap is important as it controls the shape of the point-spread function, which changes from a dual lobe structure to a single lobe, when displacing the foci along the optical axis [6]. The dual lobe structure may be of special interest when measuring the dynamics of single gold nanoparticles in solution since it introduces a second length

scale which is the separation of the two lobes and therefore allows to follow the dynamics along the optical axis [6].

Figure 5 sketches the possible modes of operation of this TwinPhoCS focal volume together with a typical time trace of a photothermal signal for 30 nm gold nanoparticles in water. The signal shows positive and negative values due to the special two-lobe structure. The structure of the signal now allows to calculate the photothermal signal autocorrelation function of the positive signals, the negative signals and the cross correlation between the positive/negative and negative/positive signals. All these individual correlation functions deliver the dynamics in the positive or negative signal lobe as well as the motion from the positive to the negative or from the negative to the positive signal lobe [6]. The latter one provides information on the dynamics due to radiation pressure.

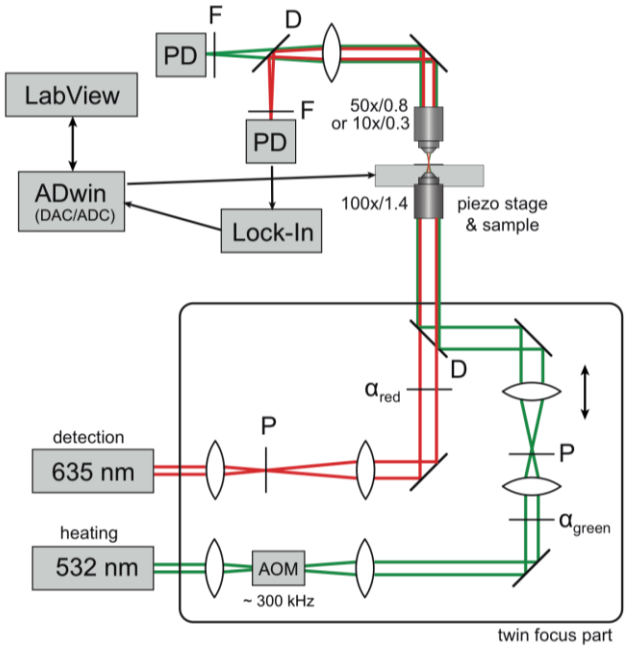

Figure 4: Photothermal single particle detection setup. PD, photodiode; P, pinhole; D, dichroic mirror; F, filter; AOM, accusto-optic modulator; α, variable ND filter; ADC, Adwin analog digital converter.

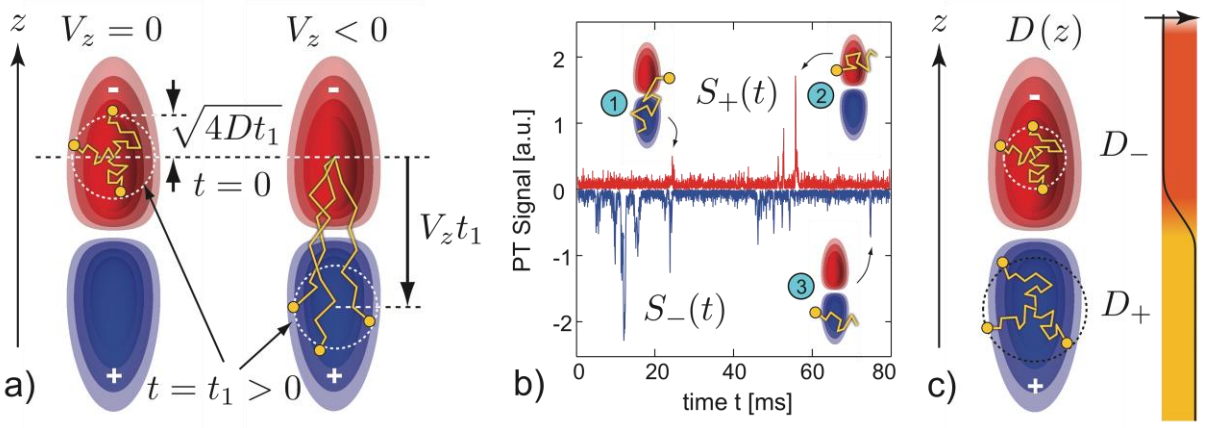

Figure 5: (a) Schematic representation of the photothermal twin-focus and a defusing species in absence ($V_z = 0$) and presence ($V_z < 0$) of an axial flow. (b) Exemplary time-trace of the positive (S_+) and negative (S_-) parts of the phase-sensitive relative photothermal signal of diffusing AuNPs. (c) The twin-focus may be used to gain spatial information on layered mobility profiles $D(z)$, since both signal contributions can be analyzed separately.

a) Size dependence of hot Brownian motion

Following the description of the absorption cross section above (section 2), it turns out that the corresponding effective diffusivity at fixed laser power exhibits an unconventional particle-size-dependence. While the conventional equilibrium Stokes–Einstein relation predicts an inverse size dependence for the diffusion coefficient of a Brownian particle, thus rendering larger particles to be slower diffusing than smaller ones, this size dependence can be very different for HBM. The size dependence of the HBM of gold nanoparticles of different size ranging from 14 nm to 46 nm radius has been measured by twin-focus photothermal correlation spectroscopy as described above (section 3). Figure 6 shows some example correlation function of the autocorrelation of the positive and the negative signal time traces as well as the cross correlation of both. The positive and negative signal time traces allow for the determination of the diffusion times through the focal volumes of the individual lobes. The cross correlation allows the measurement of the direction and speed of the radiation pressure induced motion [6]. The corresponding radiation pressure induced directional motion is found to be on the order of a few 10 nm per ms and depends almost linearly on the heating power. The diffusion time and thus the diffusion coefficient of the particles do also depend almost linearly on the heating power as demonstrated earlier [6].

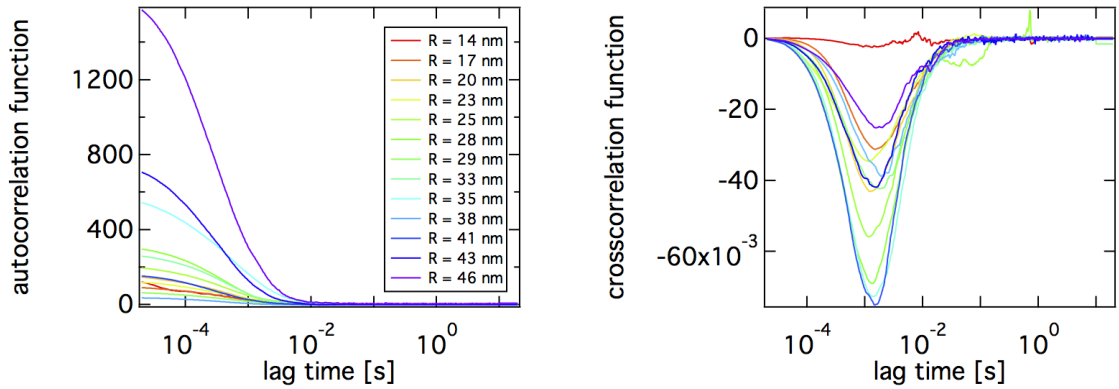

Figure 6: (left) Photothermal signal autocorrelation function particle sizes $R = 14, ..., 46$ nm at an incident heating power of $P = 1.5$ mW at the entrance aperture of the microscope objective. (right) Photothermal signal crosscorrelation functions for the particle sizes of the left graph.

The size dependence of the particle diffusion coefficient at constant heating power is revealed in Figure 7 together with the theoretical predictions according to the absorption cross section and the theory of hot Brownian motion. Since the heating intensity is non-uniform in the detection volume, the tracer's temperature will change by diffusing through the focus. Thus the temperature has to be averaged over the focus and the expected diffusion coefficient gives a much weaker reversed size dependence (see Figure 7, red curve). The experimental results roughly follow the predicted behavior. A slight increase in the diffusion coefficient is observed at particle radii larger than 40 nm as predicted. The scattering of the data points is, however, too large to assign this trend with confidence. The reason for this scattering is to some extent based on the change in the dual lobe structure of the twin focus detection volume. This effect is clearly visible by studying the photothermal signal distribution [12] and can be explained by the fact that with increasing particle size, the gold nanoparticle itself acts like a modulated scatterer.

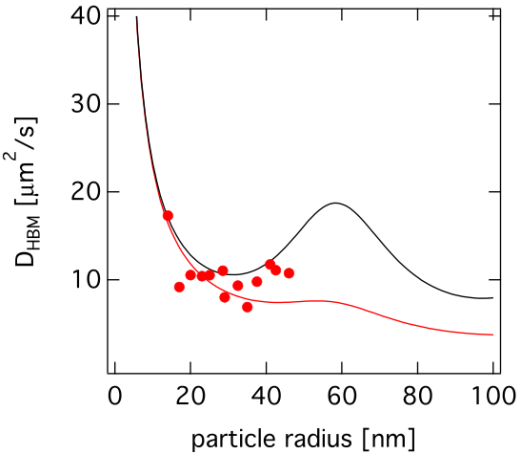

Figure 7: Comparison of the size-dependent hot Brownian motion of gold nanoparticles in water for a uniform temperature (black curve) and an averaged 3D Gaussian temperature distribution in the heating laser focus (red curve) [13].

b) Molecular dynamics simulations of hot Brownian motion and hot Janus particles

As shown above, in Figure 3 (right), we tested our theoretical predictions numerically, using non-equilibrium molecular dynamics simulations of solid nanoparticles suspended in a Lennard-Jones fluid [2, 3]. Further, as an extension of our results to a more complex and very interesting application, we considered hot Janus particles (see Figure 8). Due to the symmetry-breaking in their design, these particles are heated heterogeneously and therefore create an anisotropic temperature gradient in the surrounding solvent. As a consequence, they perform self-phoretic directed motion along their symmetry axis when heated, e.g. by laser light. On large scales, this self-propulsion manifests itself in a hugely increased diffusion coefficient. On a more local scale the motion is found to be on average of a ballistic nature (due to the self-propulsion) with translational and rotational hot Brownian motion superimposed.

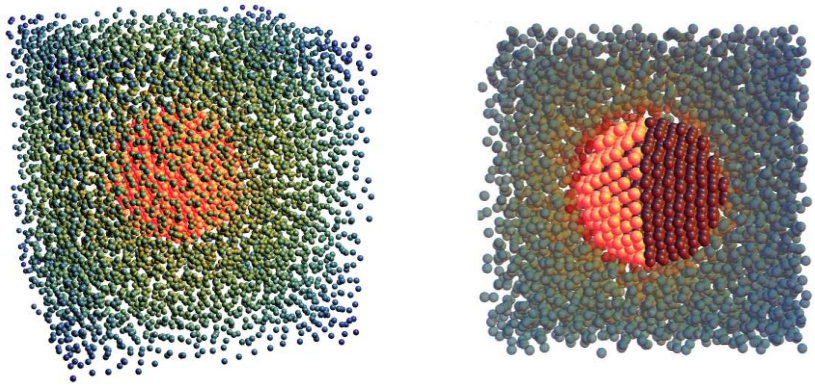

Figure 8: Snapshots from the simulation. To test our theoretical predictions, we performed massively parallel non-equilibrium molecular dynamics (NEMD) simulations of hot Brownian particles on graphics processing units (GPUs). (left) A hot nanoparticle performing hot Brownian motion. (right) A hot Janus particle simultaneously performing hot Brownian motion and “active” self-thermophoretic motion.

After a certain characteristic distance, the direction of the particle trajectory is randomized, due to the hot rotational Brownian motion. We find that, to a good approximation, the effective temperature of this randomizing motion can be estimated by the analytical formula for the rotational hot Brownian temperature, evaluated at the average temperature of the particle (see Figure 9). Corrections resulting from the anisotropic viscosity, solvent velocity field and dissipation integral can be estimated to be

relatively small for moderate heating, but might be detectable by numerical precision measurements in future simulations.

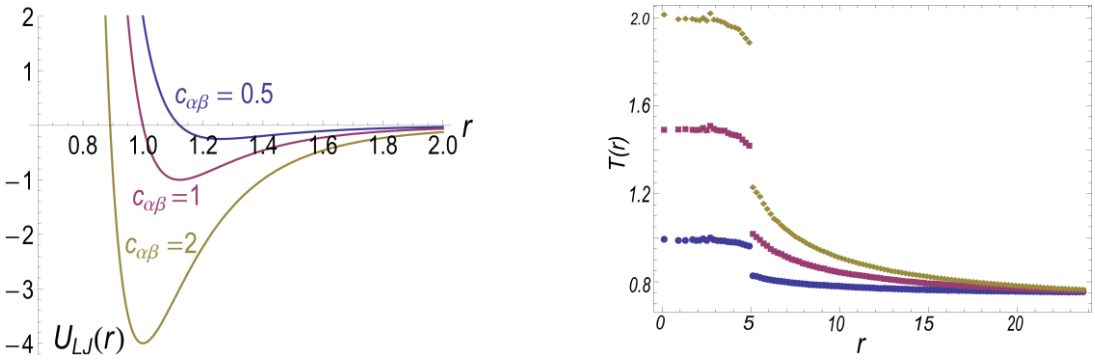

Figure 9: (left) The modified Lennard-Jones potential for three values of the wetting parameter. The minimum of the potential changes with the choice of the wetting parameter $c_{\alpha\beta}$. For $c_{\alpha\beta} = 0$, the attractive part of the potential vanishes, for $c_{\alpha\beta} = 2$ the minimum of the potential is located at $r_0 = \sigma$. (right) The radial temperature field measured from the center of a homogeneous colloid, which is heated to three different temperatures: 1.0 (circles), 1.5 (squares) and 2.0 (diamonds). The discontinuity of the temperature field at the solid-fluid boundary is due to the thermal Kapitza resistance and sensitive to the potential parameters of fluid and solid.

Our model system consists of a single colloidal particle immersed in a Lennard-Jones fluid, as depicted in Figure 8. The colloid is constructed from a spherical cut of an FCC lattice made of Lennard-Jones particles that are bound together by FENE potential, $U(r) = -0.5\,\kappa\,R_0^2 \log(1 - (r/R_0)^2)$. Distances, energy and time are measured in LJ-units of σ, ϵ and $\tau = \sqrt{m\sigma^2/\epsilon}$, respectively. Periodic boundary conditions are imposed on all three directions of the simulation box. The complete system, consisting of the particle and the Lennard-Jones solvent is equilibrated in the NPT ensemble using a Nosé–Hoover thermostat and barostat at an equilibrium pressure of $P_0 = 0.01\,\epsilon/\sigma^3$ and temperature of $T_0 = 0.75\,\epsilon/k_B$. After an initial equilibration, the atoms of the colloid are heated using a velocity-rescaling scheme that conserves the total system momentum. A similar rescaling is applied to the solvent particles near the boundaries of the simulation box to keep them at the ambient temperature. Upon heating of a homogeneous colloidal particle a symmetric temperature field develops that depends only on the radial distance from the center of the colloid. Once a steady state is reached, we start recording our measurement data.

To realize the broken symmetry of a Janus particle in our simulation, we employ a slightly modified Lennard-Jones potential given by $U_{\alpha\beta}(r) = 4\,\epsilon\left[(\sigma/r)^{12} - c_{\alpha\beta}(\sigma/r)^6\right]$, where the parameter $c_{\alpha\beta}$ takes values between 0 and 2 to account for unequal solvent interactions of the bulk and the cap of the Janus particle. A plot of the potential is shown is Figure 9 (left). A thin layer of atoms in the upper hemisphere of the colloid is identified as the cap (which is made of gold in the experiments) and has the wetting parameter denoted by c_{gs}. The rest of the colloid represents the bulk material (polystyrene in the experiments) with a wetting parameter c_{ps}. Due to different acoustic speeds in the solid and fluid regions, and due to the diverse wetting efficiencies of the cap and bulk, there appear different interfacial thermal resistances at the solid-fluid interfaces. They manifest themselves as discontinuities in the temperature field across the solid-fluid interface (see Figure 9 right). The thermal resistance is largest when $c_{\alpha\beta} = 0$

and least when $c_{\alpha\beta} = 2$. We exploit this microscopic phenomenon in generating the self-propulsion of the Janus particle.

The solvent temperature field tangential to the particle surface is shown in Figure 10 (right). The temperature gradient along the surface of the Janus particle generates a directed phoretic motion of the colloid. In a body frame rotating with the particle, the phoretic and hot Brownian translational motion decouples from the hot Brownian rotational motion. Therefore, the motion perpendicular to the direction of propulsion is purely diffusive while the motion parallel to the symmetry axis of the Janus particle exhibits a ballistic component at longer times (see Figure 10 left).

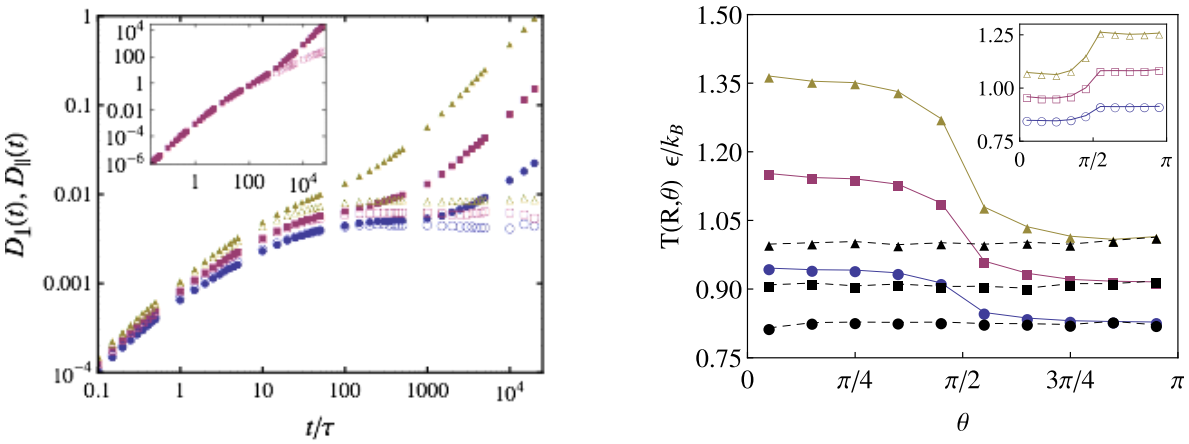

Figure 10: (left) NEMD simulation of a heated spherical Janus bead. Displayed is the time dependent diffusivity, corresponding to the particle's mean-square displacement (inset) per time parallel (filled symbols) and perpendicular to the particle's symmetry axis for three temperatures of the hot cap: in LJ units 1.1 (blue), 1.5 (red), and 2.0 (green). The wetting parameter of the cap is twice that for the bulk particle. (right) Fluid temperature profile on the surface of a heated Janus particle for parameter values $c_{\mathrm{gs}} = 2$, $c_{\mathrm{ps}} = 1$ and $c_{\mathrm{gs}} = 1$, $c_{\mathrm{ps}} = 2$ (inset). The corresponding black points are the fluid temperature on the surface of a heated colloid without any broken symmetry. The corresponding temperatures of the nanoparticle were $T_{\mathrm{p}} = 1.00\ \epsilon/k_{\mathrm{B}}$ (●, ○, ●), 1.25 ϵ/k_{B} (■, □, ■) and 1.50 ϵ/k_{B} (▲, △, ▲). The lines are guide to the eye.

4 Self-thermophoretic microswimmers

a) Self-propulsion by asymmetric temperature profiles

While the heating of spherical gold nanoparticles allows the enhancement of the diffusivity due to the increase in temperature and the decrease in viscous friction, a persistent directed motion cannot be achieved due to the spherical symmetry of the temperature field. We have thus explored the generation of an asymmetric temperature profile around a spherical particle to yield directed motion. Using an asymmetric temperature profile leads to temperature gradients tangential to the surface that induce a persistent directed motion of the particle [14]. Coating a hemisphere of a polymer particle with a thin gold layer, which can be heated by a resonant laser may create such asymmetric temperature profiles.

Figure 11 shows on the left side an electron microscopy image of such a Janus particle. As the gold layer efficiently absorbs light, it heats up and results in an asymmetric temperature profile along the surface of the particle as shown in Figure 11 (right) [14, 15]. The temperature gradient tangential to the surface induces a variation in the interaction energy of the solvent with the particle surface, which is different from the bulk and thus results in a creep flow along the surface. This creep flow can be regarded as a slip hydrodynamic boundary condition with a slip velocity $\vec{v}_{\mathrm{s}} = \mu \nabla T$ causing a complex flow profile

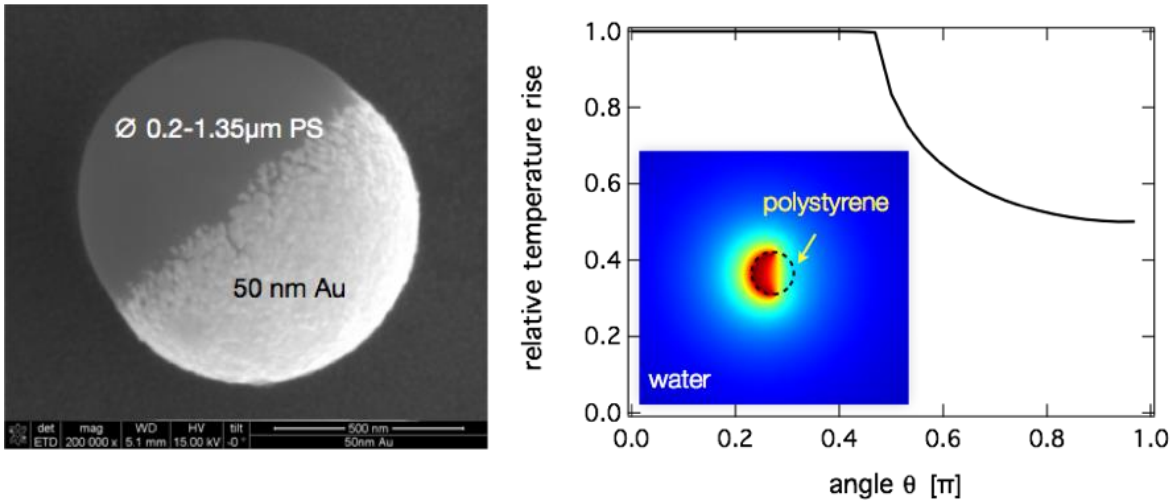

Figure 11: (left) Electron micrograph of a 1 µm polystyrene particle with a 50 nm gold layer. (right) Relative temperature profile along the circumference of the Janus particle as calculated in finite element simulations. The inset shows the temperature map around the particle in water. The dashed line indicates the boundary of the Janus particle to the water.

around the particle and a propulsion velocity, which is

$$\vec{v}_{\mathrm{T}} = -D_{\mathrm{T}}\nabla T, \tag{6}$$

where

$$D_{\mathrm{T}} = -\frac{2}{3}\mu. \tag{7}$$

As the slip flow is typically from the cold to the hot side of the particle, the particle itself is propelled in the opposite direction with the polymer side leading. The overall motion is now determined by the propulsion speed and the rotational and translational Brownian motion which leads to a mean square displacement according to

$$\langle \Delta r^2(\Delta t)\rangle = 4D\Delta t + \frac{v^2\tau_R^2}{2}\left[\frac{2\Delta t}{\tau_R} + e^{-2\Delta t/\tau_R} - 1\right]. \tag{8}$$

These phoretic swimmers therefore fit into the general framework of phoretic swimmers as described earlier for example by Howse et al. [16] except that the propulsion is not fueled chemically but by the laser heating of the gold cap.

b) Experimental setup

The propulsion of such photophoretic Janus particles has been studied using the setup displayed in Figure 12. The gold cap of the microswimmers is continuously illuminated by a laser beam with a wavelength of 532 nm. The heating laser light is focused into the sample area by an oil immersion microscope objective with adjustable numerical aperture Olympus (100x/NA0.6-1.3) to yield an illuminated area of about 10 × 10 µm^2. The Janus swimmers are imaged using white light under dark field illumination by a dark field condenser. The scattered light of the Janus particle is collected by the same microscope objective as used for the heating.

The resulting dark field microscopy image is detected by an EM-CCD camera (Andor IXON) with an inverse framerate of 15 ms. The particle position is tracked in real time using LabView (National Instruments Inc.) and sent back to a piezo stage controlling the sample position. The feedback mode allows to keep the position of the Janus particle fixed with respect to the heating beam intensity maximum, thus ensuring a temporally constant heating power. The piezo positions as well as the residual motion of the Janus microswimmers in the recorded images are used to reconstruct the trajectories of the swimmers to calculate their mean square displacement and other quantities.

The home-built microfluidic cells (Figure 12 right), composed of two glass slides with a vertical spacing of a few micrometers ensured by non-cross-linked silicone, require previous surface passivation in order to prevent sticking of particles; commonly the nonionic block copolymer Pluronic F127 was used.

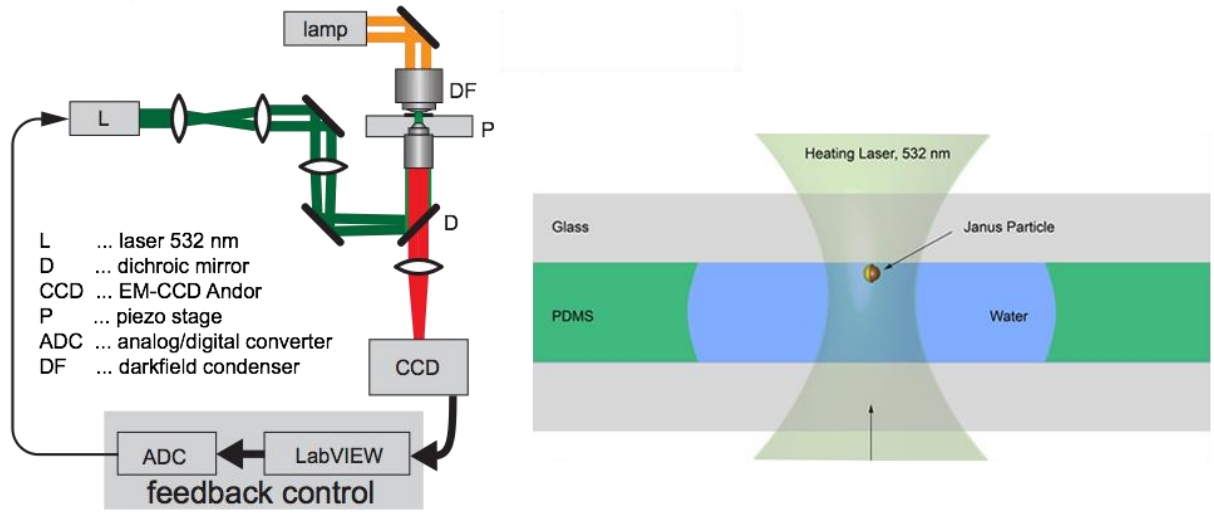

Figure 12: (left) Schematics of the experimental setup for the study of self-thermophoretic Janus-microswimmers. (right) Scheme of the sample cell consisting of two glass cover slides, which are surface modified with Pluronic F127. The cover slides confine a thin water film of less than 2 µm thickness. The water film is sealed by a thin silicon oil film at the edges of the sample.

c) Results

As depicted in Figure 13 (left) for a Janus particle of 2 µm diameter and at different heating powers, the mean square displacement (MSD) of the Janus particles exhibits a nonlinear time dependence. The initial part of the MSD shows a quadratic dependence corresponding to a ballistic motion of the swimmer. Since the particle still carries out translational and rotational Brownian motion, the initial ballistic part changes into an effective diffusive motion at longer times with a linear time dependence of the MSD. This leads to an effective diffusive motion with an effective diffusion coefficient according to the propulsion velocity v and the rotational diffusion time τ_R. The particles propulsion velocity scales linearly with the heating power and inversely with the viscosity as depicted in Figure 13 (middle). The direction of this active motion can be inferred from the orientational correlation. This correlation projects the displacement vector between two successive frames of a time series onto the orientation of the particle. As depicted in Figure 13 (right), the correlation decays exponentially with the rotational correlation time and is negative due to the definition of the particle direction and the fact that the particles polymer side presents the leading side of the directed motion.

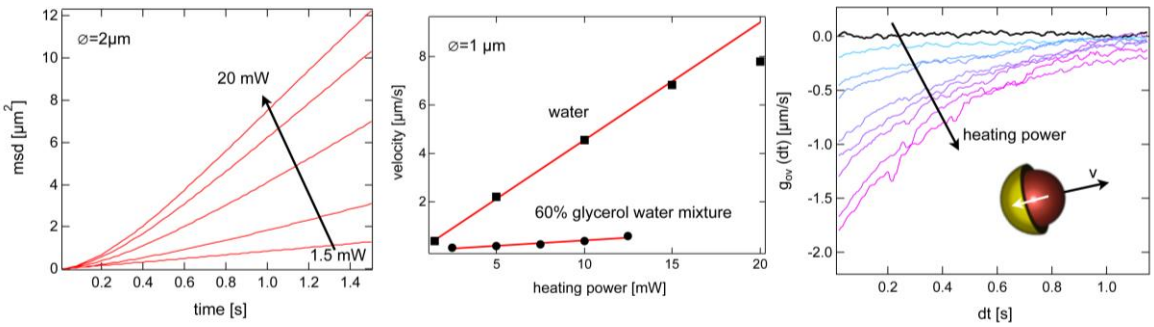

Figure 13: (left) Mean square displacement of a $\varnothing = 2$ µm Janus particle as a function of time at different incident laser powers. The heating laser illuminates an area of 10×10 µm^2. (middle) Propulsion velocity of a $\varnothing = 1$ µm Janus particle in water and a 60 % glycerol/water mixture. (right) Correlation function of the particle displacement vector and the orientation of the particle according to the inset definition.

The contribution of hot Brownian motion to the particle dynamics can be revealed by measuring the rotational diffusion time and the translational diffusion coefficient as a function of the heating power. As displayed by Figure 14 the rotational and translation diffusion is nearly unchanged when increasing the heating power.

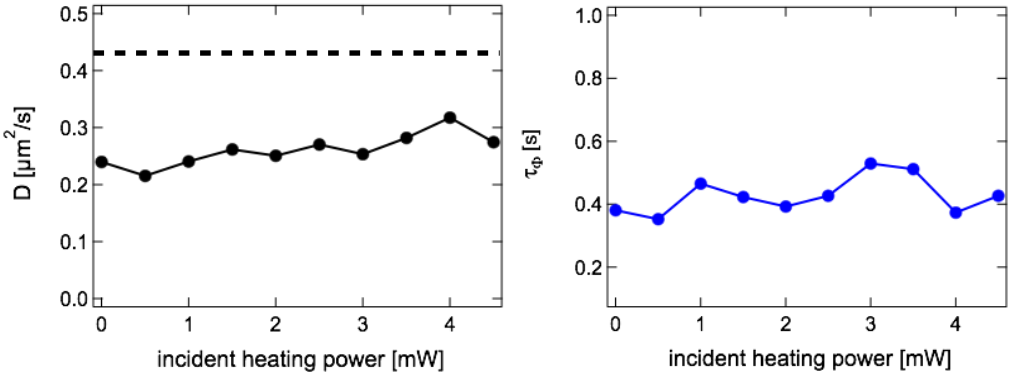

Figure 14: (left) Diffusion coefficient of a $\varnothing = 1$ µm Janus particle as a function of the heating power. The diffusion coefficient is extracted from the distribution of particle displacements between two subsequent frames ($\Delta t = 10$ ms). The dashed line corresponds to the expected value according to the Stokes–Einstein relation using the viscosity of water. (right) Rotational diffusion time of the Janus particle as determined from the $\varnothing = 1$ µm in plane orientation of the Janus particles in water.

In summary, the prepared Janus particles show a directed motion when heated with an incident laser. This motion of the Janus particles has been characterized and is comparable to other systems using diffusiophoresis based on catalytic chemical reactions [16–19]. The presented self-propulsion mechanism can be switched on and off by switching the heating laser. The propulsion mechanism is not running out of fuel as compared to the chemically propelled particles and it requires no special medium as thermophoresis occurs with variable strength in all systems. Using these advantages, we have developed a steering mechanism for the Janus swimmers [15, 20]. The technique employs a real-time feedback of the particle position and orientation to switch the propulsion only in cases where the particle orientation points towards a specific target. This so-called photon nudging procedure has been shown to scale favorably with the particles size as rotational and translational Brownian motion of the Janus particles scale differently with the particle radius (rotation with inverse volume, translation with the inverse radius). Photon nudging is thus harnessing the rotational fluctuations to localize and manipulate individual particles [15, 20].

5 Construction of DNA templated thermophoretic swimmers

In general, besides the intended propulsion, phoretic microswimmers experience both thermal translational and rotational diffusion, the latter randomizing the direction of motion. This effect can be conquered by confining the motion to predetermined tracks or by external reorientation. A new approach is the manipulation of individual microswimmers by adaptive photon nudging [15, 20].

The mean-squared displacement (MSD) of a self-propelled particle with a velocity as given above. Therefore, control of the rotational diffusion, in particular an increase of the rotational relaxation time would improve the directional motion, since then the contribution of the propulsion becomes more significant [16]. An increase of the rotational relaxation time is achievable in several ways:

i) by simply using larger particles, since the rotational diffusion time scales with the particle volume,
ii) by surface confinement effects forcing the particles in a particular orientation due to i.e. hydrodynamic interactions with the interface or, what was focused on in this work,
iii) by attaching elements that suppress rotational motion and stabilize the motion.

Here, the behavior of thermophoretic microswimmers basically consisting of a thermally active Janus particle (JP) and long double-stranded DNA (dsDNA) was investigated. The Janus particles are micrometer-sized polystyrene beads having one hemisphere coated with a 50 nm thin gold layer as described in section 4a. The contour length of the applied dsDNA was in the order of a few micrometers, which, taking a persistence length of about 50 nm into account, results in a micrometer-sized entropic DNA-coil.

The parameter, characterizing the thermophoretic properties of the constituents is the Soret coefficient S_T, describing the ratio of thermodiffusion D_T and the Brownian diffusion D. For micrometer-sized polystyrene beads and 16 µm long dsDNA in bulk, the Soret coefficient is in the order of 10 K^{-1} and 1 K^{-1}, respectively. The Soret coefficient of dsDNA with a contour length L scales with $L^{1/2}$ [21].

Optically heating the Janus particles with a laser beam leads, due to light absorption on the gold side, to an asymmetric temperature profile around the particle that in turn results in a flow field surrounding and finally driving the particle. Double-stranded DNA was attached to the gold side of the Janus particle expecting several effects: i) stabilization of the Janus particle propulsion reflected in enhanced directional motion and ii) impact on the thermophoretic velocity of the Janus particle due to thermophoretic stretching of the DNA in the temperature gradient [22, 23].

Hybrids of thermo-active Janus particles and rigid DNA origami structures (Figure 15a) have been realized. As DNA origami structures so called six-helix-bundles (6HB) with a length of 400 nm and a persistence length of 1.8 µm [24] were used. Further, DNA was used as a linker to connect micrometer-sized polystyrene cargo beads and Janus particles (Figure 15b) extending the initial goal to even more elaborated constructs. This allows not only for control of rotational diffusion but also for intrinsic force determination.

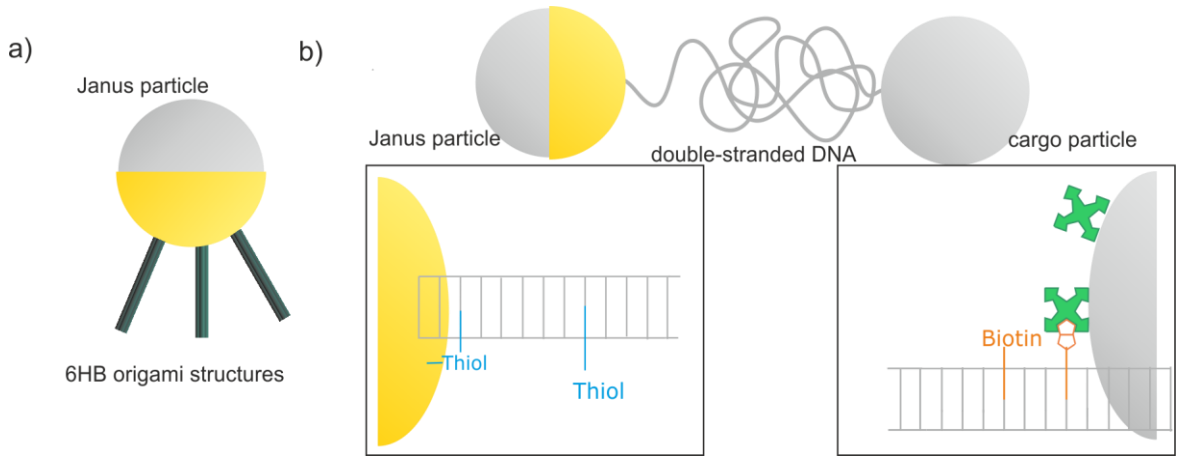

Figure 15: Hybrids of Janus particles and DNA elements for control of the rotational diffusion (a) stiff DNA origami tubes (6HB) and (b) a cargo bead is linked by a dsDNA molecule.

In order to attach dsDNA of different lengths specifically to the gold side of the Janus particle, functional groups had to be integrated at the molecules ends. DNA-lengths of 16.3 µm (λ-phage DNA), 8.1 µm (λ/2-DNA) and 3.3 µm have been studied. λ-phage DNA is commercially available, λ/2-DNA was achieved by using the restriction enzyme X*ba*I for bisecting λ-phage DNA. DNA with a length of 3.3 µm has been synthesized applying polymerase chain reaction (PCR). λ-phage DNA and λ/2-DNA possess single-stranded (ss) overhangs that can be enzymatically filled in with nucleotides carrying functional groups such as biotin or thiol using *Klenow* polymerase in a one-step procedure.

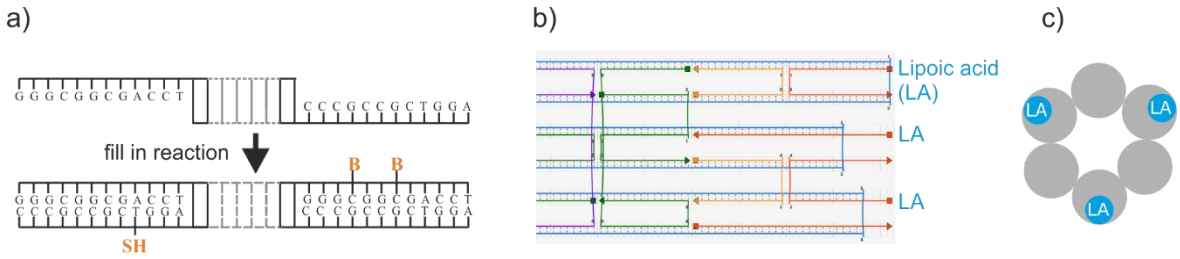

Figure 16: (a) λ-DNA is functionalized with biotin (B) and thiol group (SH) by filling-in the single-stranded overhangs. (b) The end of the 6HB origami tube contains 3 staples carrying functional groups (lipoic acid) for rigid and perpendicular binding to particles. (c) Front view of the 6HB displaying the symmetrical arranged functional groups.

The incorporation of different functional groups on either side (Figure 16a) requires several fill-in steps. For the PCR product of 3.3 µm length, the single-stranded overhangs were generated by restriction digestion with the enzyme A*pa*I and subsequently filled in following a similar procedure.

The rigid six-helix-bundle (6HB) origami structure is based on the CaDNAno design of M. Wiens [25]: the template strand (M13mp18, 7249 bases long) is folded in the target structure by 176 staple strands of which three, situated at the tubes end, carry lipoic acid (Figure 16b). In order to achieve rigid and perpendicular binding to the Janus particles a tripod structure as depicted in Figure 16c was chosen. Compared to thiol groups, lipoic acid (also thioctic acid) offers a longer-term stability.

As cargo particles, polystyrene spheres with a diameter of 1 µm have been used; functionalization of the bead surface with streptavidin for binding to the biotinylated DNA molecules was realized by a standard EDC/NHS procedure.

Upon binding of DNA or DNA based origami structures to Janus particles, the hybrid formation was verified using transmission electron microscopy (TEM). Energy filtering (EFTEM) allowed a clear distinction between the two sides of the Janus particles (Figure 17a). Depending on the experimental conditions, binding of single molecules (Figure 17b) or DNA bundles could be achieved; due to capillary forces during TEM sample preparation, dsDNA is stretched. Also the attachment of 6HB origami structures on Janus particles with a diameter of 700 nm is detectable (Figure 17c).

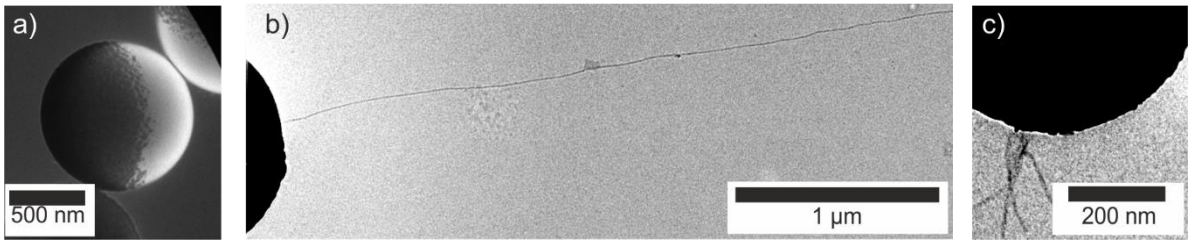

Figure 17: TEM micrographs of Janus particles. (a) Energy filtering enables to distinguish the different hemispheres. (b) A single DNA molecule and (c) DNA origami tubes are attached.

Figure 18 depicts the difference in the thermophoretic behavior of bare and DNA-modified Janus particles. Optical heating of bare Janus particles results in a stronger diffusion (Figure 18a), heating Janus particles with attached long dsDNA leads to a more directed motion (Figure 18b). As argued before, the rotational relaxation time, as the parameter characterizing the rotational diffusion, is increased for hybrids of Janus particles and DNA due to at least two effects: 1. the larger size of the hybrid compared to bare Janus particles and 2. the partial uncoiling of the DNA due to thermophoretic stretching that additionally stabilizes the motion against rotations. The influence of the longer DNA molecules (8.1 µm) on the rotational relaxation time is with increasing laser power larger (Figure 19a). Between 15 mW and 20 mW heating power a strong increase of the rotational diffusion time for the 8.1 µm long DNA is observed, which suggests a threshold power for the stretching of the DNA in the temperature field of the gold cap. This is largely absent for the 3.3 µm DNA, which suggests that the mechanism of rotational slow down is simply due to the coiled DNA at the gold cap surface increasing the volume.

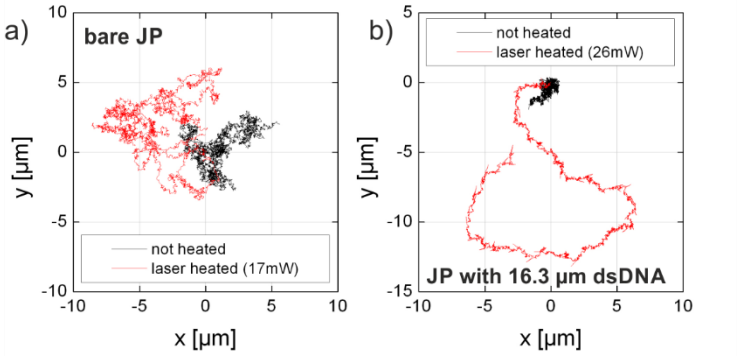

Figure 18: Trajectories of heated and unheated Janus particles: (a) A bare JP shows diffusive behavior in both cases. (b) If DNA is attached to the JP; the motion becomes more directed in case of heating.

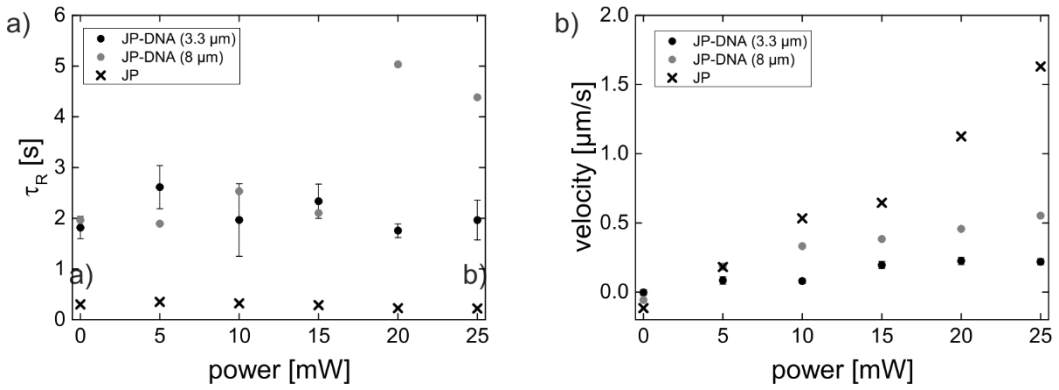

Figure 19: (a) Rotational relaxation time versus heating power demonstrates the impact of the DNA modification on the rotational diffusion. (b) Thermophoretic velocity versus heating power shows the expected velocity rise with increased heating. The DNA modified hybrids show a nonlinear increase.

The thermophoretic velocity (Figure 19b) rises with increased heating as expected; comparing bare Janus particles and DNA-modified ones for similar laser power reveals a smaller and nonlinear velocity increase for the latter. Currently it is not clear, why the velocity of the hybrids with the longer DNA molecules is slightly larger than for the shorter ones. Effects that have to be taken into account are the dependency of the Soret coefficient on the conformation of the DNA, the modification of the actual interaction layer in which the phoretic flow field builds up and the particular binding site of the DNA. All of these details are currently not yet well controlled and may contribute to a modified propulsion velocity, which also creates nonlinearity i.e. due to a stretching of the DNA.

6 Conclusion

Different types of optically heated particles have been studied to explore the influence of a steady state temperature field on the motion of a Brownian particle. Heated gold nanoparticles have been used to reveal the influence of a radially symmetric temperature profile around the nanoparticle. The results show that the diffusive motion, which is termed hot Brownian motion, can be described by an effective temperature as well as with an effective friction for each degree of freedom. These effective quantities allow a description of hot Brownian motion in terms of a fluctuation dissipation relation similar as for the isothermal case, but somewhat less universally. It has also been shown that due to the size dependence of the absorption cross section of the gold nanoparticles a new unusual size dependence of the hot Brownian motion is observed at fixed illumination, which deviates from the expected inverse size dependence of the Stokes–Einstein law.

Asymmetric temperature profiles have been demonstrated to introduce self-thermophoretic propulsion into the motion of micronized objects. The prepared Janus-swimmers with a polymer microparticle core and a gold cap show propulsion speed of a few ten micrometers per second, which are the result of a tangential temperature gradient along the surface of the Janus particle. While the motion of the Janus-swimmer is directed at short times, it gets randomized in direction by the rotational diffusion of the particle. To stabilize this rotational motion, we have coupled the Janus-particles to DNA structures. These DNA structures are made of dsDNA or DNA origami and can be used to form even more complex structures of multiple Janus swimmers. First experimental results demonstrate how the

propulsion speed as well as the rotational diffusion of the Janus swimmer hybrids is modified by the presence of the DNA structures.

Acknowledgements

The research reported in the manuscript has been supported by the Deutsche Forschungsgemeinschaft within project P1 “Hot Brownian motion” of the Saxon Research Unit FOR 877 “From Local Constraints to Macroscopic Transport”. D.C. acknowledges funding from Science and Engineering Research Board (SERB), India vide fund no. SB/S2/CMP-113/2013.

References

[1] D. Rings, R. Schachoff, M. Selmke, F. Cichos, K. Kroy: *Hot Brownian motion.* Phys. Rev. Lett. **105**, 090604 (2010)

[2] D. Chakraborty, M.V. Gnann, D. Rings, J. Glaser, F. Otto, F. Cichos, K. Kroy: *Generalised Einstein relation for hot Brownian motion.* EPL **96**, 60009 (2011)

[3] D. Rings, D. Chakraborty, K. Kroy: *Rotational hot Brownian motion.* New J. Phys. **14**, 053012 (2012)

[4] G. Falasco, M.V. Gnann, D. Rings, K. Kroy: *Effective temperatures of hot Brownian motion.* Phys. Rev. E **90**, 032131 (2014)

[5] D. Rings, M. Selmke, F. Cichos, K. Kroy: *Theory of hot Brownian motion.* Soft Matter **7**, 3441–3452 (2011)

[6] M. Selmke, R. Schachoff, M. Braun, F. Cichos: *Twin-focus photothermal correlation spectroscopy.* RSC Adv. **3**, 394–400 (2013)

[7] C.F. Bohren, D.R. Huffman: *Absorption and scattering of light by small particles*. Wiley-Interscience (1998)

[8] A. Gaiduk, M. Yorulmaz, P.V. Ruijgrok, M. Orrit: *Room-temperature detection of a single molecule's absorption by photothermal contrast.* Science **330**, 353–356 (2010)

[9] D. Boyer, P. Tamarat, A. Maali, B. Lounis, M. Orrit: *Photothermal imaging of nanometer-sized metal particles among scatterers.* Science **297**, 1160–1163 (2002)

[10] M. Selmke, M. Braun, F. Cichos: *Photothermal single-particle microscopy: Detection of a nanolens.* ACS Nano **6**, 2741–2749 (2012)

[11] R. Radünz, D. Rings, K. Kroy, F. Cichos: *Hot Brownian particles and photothermal correlation spectroscopy.* J. Phys. Chem. A **113**, 1674–1677 (2009)

[12] M. Selmke, M. Braun, R. Schachoff, F. Cichos: *Photothermal signal distribution analysis (PhoSDA).* PCCP **15**, 4250–4257 (2013)

[13] D. Rings: *Hot Brownian motion*. PhD Thesis, Universität Leipzig (2013)

[14] H.-R. Jiang, N. Yoshinaga, M. Sano: *Active motion of a Janus particle by self-thermophoresis in defocused laser beam.* Phys. Rev. Lett. **105**, 268302 (2010)

[15] B. Qian, D. Montiel, A. Bregulla, F. Cichos, H. Yang: *Harnessing thermal fluctuations for purposeful activities: The manipulation of single micro-swimmers by adaptive photon nudging.* Chemical Science **4**, 1420–1429 (2013)

[16] J.R. Howse, R.A.L. Jones, A.J. Ryan, T. Gough, R. Vafabakhsh, R. Golestanian: *Self-motile colloidal particles: From directed propulsion to random walk.* Phys. Rev. Lett. **99**, 048102 (2007)

[17] W.F. Paxton, K.C. Kistler, C.C. Olmeda, A. Sen, S.K. St. Angelo, Y. Cao, T.E. Mallouk, P.E. Lammert, V.H. Crespi: *Catalytic nanomotors: autonomous movement of striped nanorods.* J. Am. Chem. Soc. **126**, 13424–13431 (2004)

[18] J.G. Gibbs, Y.-P. Zhao, J.G. Gibbs, Y.- Zhao: *Autonomously motile catalytic nanomotors by bubble propulsion.* Appl. Phys. Lett. **94**, 163104 (2009)

[19] L.F. Valadares, Y.G. Tao, N.S. Zacharia, V. Kitaev, F. Galembeck, R. Kapral, G.A. Ozin: *Catalytic nanomotors: Self-propelled sphere dimers.* Small **6**, 565–572 (2010)

[20] A.P. Bregulla, H. Yang, F. Cichos: *Stochastic localization of microswimmers by photon nudging* ACS Nano **8**, 6542–6550 (2014)

[21] S. Duhr, D. Braun: *Why molecules move along a temperature gradient.* PNAS **103**, 19678–19682 (2006)

[22] H.-R. Jiang, M. Sano: *Stretching single molecular DNA by temperature gradient.* Appl. Phys. Lett. **91**, 154104 (2007)

[23] J.N. Pedersen, C.J. Lüscher, R. Marie, L.H. Thamdrup, A. Kristensen, H. Flyvbjerg: *Thermophoretic forces on DNA measured with a single-molecule spring balance.* Phys. Rev. Lett. **113**, 268301 (2014)

[24] D.J. Kauert, T. Kurth, T. Liedl, R. Seidel: *Direct mechanical measurements reveal the material properties of three-dimensional DNA origami.* Nano Lett. **11**, 5558–5563 (2011)

[25] M. Wiens: *Fabrication of linear nanoparticle arrays by DNA origami.* Master Thesis, TU Dresden (2010)